APL Materials

In-line metrology for roll-to-roll UV assisted nanoimprint lithography using diffractometry

Cite as: APL Mater. **6**, 058502 (2018); https://doi.org/10.1063/1.5011740
Submitted: 02 November 2017 . Accepted: 28 February 2018 . Published Online: 28 March 2018

Martin Kreuzer, Guy L. Whitworth, Achille Francone, Jordi Gomis-Bresco, Nikolaos Kehagias, and Clivia M. Sotomayor-Torres

In-line metrology for roll-to-roll UV assisted nanoimprint lithography using diffractometry

Martin Kreuzer,[1,a] Guy L. Whitworth,[1] Achille Francone,[1]
Jordi Gomis-Bresco,[1] Nikolaos Kehagias,[1] and Clivia M. Sotomayor-Torres[1,2]
[1]*Catalan Institute of Nanoscience and Nanotechnology (ICN2), CSIC and BIST, Campus UAB, Bellaterra, 08193 Barcelona, Spain*
[2]*Institució Catalana de Recerca i Estudis Avancats (ICREA), 08010 Barcelona, Spain*

(Received 2 November 2017; accepted 28 February 2018; published online 28 March 2018)

We describe and discuss the optical design of a diffractometer to carry out in-line quality control during roll-to-roll nanoimprinting. The tool measures diffractograms in reflection geometry, through an aspheric lens to gain fast, non-invasive information of any changes to the critical dimensions of target grating structures. A stepwise tapered linear grating with constant period was fabricated in order to detect the variation in grating linewidth through diffractometry. The minimum feature change detected was ~40 nm to a precision of 10 nm. The diffractometer was then integrated with a roll-to-roll UV assisted nanoimprint lithography machine to gain dynamic measurements *in situ*. https://doi.org/10.1063/1.5011740

The critical dimensions of nanostructures are routinely obtained by means of powerful imaging techniques such as scanning electron microscopy (SEM)[1] and atomic force microscopy (AFM).[2,3] Advanced nanofabrication technology has moved toward high-throughput, large area, and scalable nanoimprinting such as UV/thermal nanoimprint lithographies (NIL) and injection moulding systems.[4] The traditional imaging techniques mentioned above, while powerful and effective, have not been able to keep in line with these advances. Both are time consuming and require *ex situ* measurements as they cannot be directly integrated with the nanoimprinting production line. With current trends now moving toward roll-to-roll imprinting, there is an ever growing need for a fast, non-invasive method for performing critical dimension (CD) metrology which can be integrated into a roll-to-roll system.[5–9] Such a device(s) would ideally provide real-time information of film thickness and grating critical dimensions for the quality control of the nanoimprint process and rapid feedback optimisation.

An optical inspection technique is one possibility for implementing rapid measurement/inspection in roll-to-roll systems. Simple techniques such as reflection, absorption, fluorescence, and Raman spectroscopy have already been integrated into such systems for determining film thicknesses.[10] Spectroscopic techniques are especially powerful as they can provide insight into the chemical composition of a film such as ellipsometry, which is able to determine the optical constants of monolayer deposits and even provide structural information.[11–13] Scatterometric techniques are sensitive to sub-wavelength features, for example, dynamic light scattering and x-ray scattering are used to determine the shape and size of nanoparticles suspended in a liquid.[14] Scatterometry is routinely used in the semiconductor industry in the characterisation of structured surfaces, whereby the zeroth order diffraction (reflected or transmitted beams) of light is monitored as a function of wavelength or angle of incidence.[15,16] Changes in the height, width, or any other CD feature of a periodic structure alters the amplitudes of the grating's Fourier coefficients, modifying the diffraction efficiency (DE) of the device. The dependency of the DE on input parameters (e.g., wavelength) can be used to determine the CDs of an inspected structure by model-assisted, inverse problem solving.[17,18]

[a]Current address: ALBA Synchrotron Light Source, 08290 Cerdanyola del Valles, Barcelona, Spain.

Diffractometry is a subset of spatially coherent scatterometry which monitors all diffractive orders simultaneously. Similarly, there needs to be a model-assisted method whereby the relative intensities of the diffractive orders would be compared to a library of simulated data. Coherent scatterometry has great potential for detecting deviations in the critical dimensions of nanostructures[19–21] and in some cases has been shown to be more sensitive than incoherent scatterometry.[22,23] Techniques such as coherent Fourier scatterometry usually require a high NA microscope objective. This can create some practical problems as prior knowledge of the incident electric field is required for the simulation library, and this is very sensitive to the optical alignment and aberrations in the system.[16,24,25]

Here we present a simple diffractometer for collecting multiple spatial diffraction patterns (diffractograms) from periodic nanostructures using an aspheric lens to reduce the aforementioned aberration effects and relax the sensitivity on the alignment of the coherent scatterometry system. Diffractograms were collected from both a rigid silicon master grating and from a transparent, flexible polydimethylsiloxane (PDMS) stamp moulded from the master structure. Deviations as small as ~40 nm showed a clear change in the intensities of the diffraction peaks, demonstrating its use as a monitoring tool. A 2D model using an in-house developed finite-difference frequency-domain (FDFD) code was used to generate far-field diffraction patterns which were compared with measured diffraction patterns from SEM characterised substrates to calibrate the diffractometry for linewidth metrology. The device was then integrated directly into a roll-to-roll UV assisted nanoimprint lithography setup to monitor real-time deviations of the linewidth of the soft PDMS stamp (negative copy of the silicon master stamp). The diffractometer, as shown in Fig. 1, is made up of a collimated He-Ne laser source which is subsequently telescoped down to a spot size of ~100 μm using a circular lens (L1) and an aspheric lens (L2). The beam is directed onto a microstructured sample placed in the focal plane of the aspheric lens (L2). Figure 1(b) specifically shows the ray pathways of the collection arm of the system, highlighting the reflected 0th diffractive order mode from the sample. Off-axis beams from higher order diffraction are also collected by the system such that the full diffraction pattern is reconstructed at the Fourier plane to the sample (as depicted). A beam splitter is used to image the reflected diffraction pattern onto the CCD using a projection lens, L3. Additional beam splitters can be installed in the collection line to allow for real-space imaging, for simultaneous diffractometry and microscopy for multi-scale defect detection.

A silicon master structure was fabricated using electron beam lithography. The master structure consisted of an 80 mm long grating with a period of 6 μm. The grating ridges were fabricated with a tapered width along the length of the master, ranging from 320 nm to 470 nm in steps of

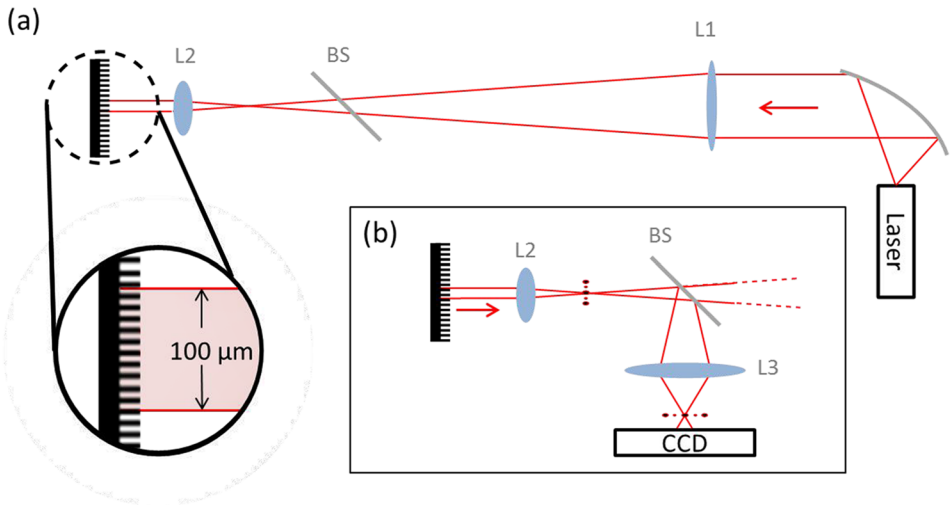

FIG. 1. Diffractometer schematic. (a) depicts exclusively the laser illumination system for illuminating the diffractive sample with a 100 μm FWHM beam. (b) shows the collection arm of the device with the ray path shown for the 0th order reflected mode. The Fourier plane to the sample is highlighted, indicated by the formation of a diffraction pattern.

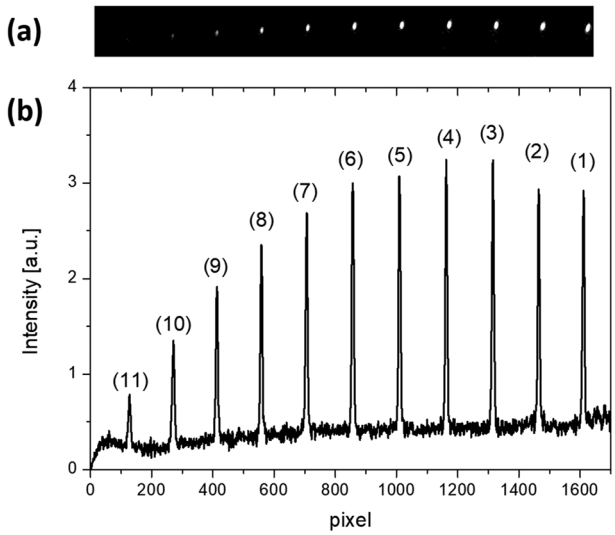

FIG. 2. (a) Example diffractogram collected from a 6 μm period silicon master grating with a linewidth of 470 nm. (b) The intensities from the diffractogram are summed and plotted as a function of CCD pixel position. Diffraction orders from 1 to 11 are indicated.

40-50 nm. After this, a large area, 3 mm thick PDMS stamp was cast from the silicon master structure to create an inverse "daughter" copy of the master structure. The PDMS was cured at 80 °C (using a 10:1 precursor:photo-initiator ratio) over 4 h.[26] The silicon master was placed in the diffractometer, capturing the diffractogram for each grating region. Figure 2(a) shows an example diffractogram collected from the grating area with 470 nm linewidth. Below in Fig. 2(b) is shown the projected pixel intensities from the diffractogram to produce a 1D diffraction pattern for easy analysis. The 4th order diffraction in Fig. 2(b) was observed to be the most intense peak; it was chosen to be monitored when scanning the critical dimension changes of the grating, having the greatest signal-to-noise ratio.

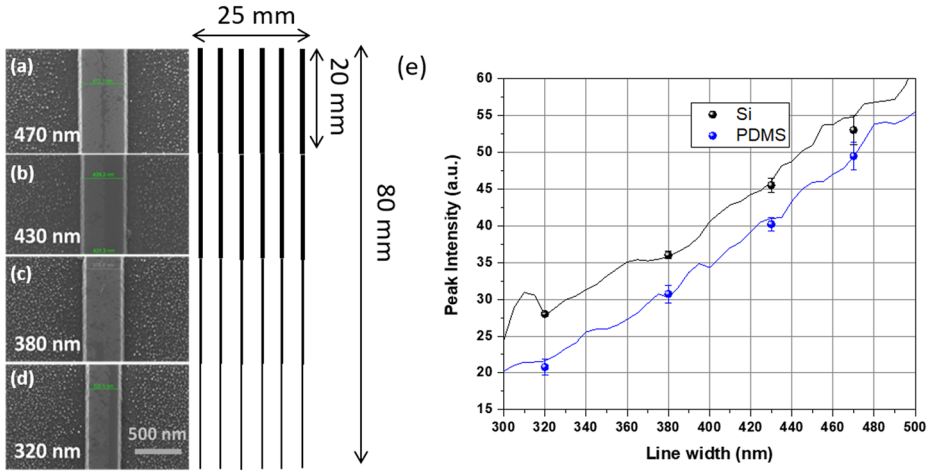

FIG. 3. [(a)–(d)] SEM images for each of the fabricated regions of the Si master structure. A simplified representation of the entire fabricated region is shown alongside. (e) Average intensity detected from the 4th order diffracted beam in reflection plotted against the linewidth of each of the sections of the grating (solid circles) with standard deviation and simulated 4th order diffractive intensities (solid-line) for silicon ridges and PDMS trenches with changing widths. The parameters used for the depicted calibration curves for Si/PDMS were a height of 115 nm/120 nm, an angle of incidence of 13°/11°, and a radius of curvature of 60 nm/40 nm. The simulated data are normalised to the respective experimental peak intensity at line width = 320 nm.

Figures 3(a)–3(d) show SEM images of the four regions of the fabricated silicon master structure. Figure 3(e) shows a plot of the beam intensity of the 4th order diffraction peak (fitted to a Lorentzian distribution) with varying linewidth of the silicon master (black) and the PDMS daughter stamp (blue). Each point represents the averaged intensity of four measurement locations with the standard deviation shown. Aside from the offset, the intensity of the diffraction peaks followed a very similar trend with changing linewidths, despite being a transparent copy of the master structure, indicating good pattern transfer.

A 2D FDFD model was built for both the silicon ridges and PDMS trenches (the inverse structure to the master) with Floquet periodic boundary conditions. The input wavelength and structural pitch in the model were fixed at 633 nm and 6 μm, respectively, as they have negligible relative error, and the sidewall angle was assumed to be 90°. The FDFD simulation was run parametrically over the height of the structures, angle of incidence, corner radius of curvature, and the four different linewidths from the SEM measurements. Each parametric run would record the near-field data, repeat it for 20 periods, and project it into the far field using an equivalence principle transformation; the resulting diffraction peak information of which was stored. The simulated 4th order diffraction peak trend was compared to the measured values in Fig. 3(e) using a χ^2 minimisation technique to determine the height, angle of incidence, and radius of curvature of the Si and PDMS structures ($\chi^2 = \sum_i (measured_i - simulated_i)^2 / simulated_i$). The measurement data was allowed to vary by up to two standard deviations to gain good statistics of the determined parameters (see Fig. S1 in the supplementary material). These parameters were then used to generate finer calibration curves to relate 4th order diffractive intensity to linewidth shown as the solid lines in Fig. 3(e). The parameters of best fit for the Si and PDMS structures were, respectively, determined to be a height of 115 ± 10 nm and 120 ± 5 nm, an angle of incidence of 13° ± 1° and 11° ± 1°, and a corner radius of 50 ± 15 nm and 40 ± 15 nm. A non-zero incidence angle was expected as the system was aligned to have as many visible diffraction spots on the CCD, and additionally an angle of >10° is needed to generate the observed 11 diffractive orders. For comparison with the arbitrary units of the experimental data, the simulated 4th order diffractive intensity was normalised to the experimental value for the 320 nm linewidth. The linewidth trends fitted very well with experimental data with low χ^2 values of $0.3 \pm 0.2 \times 10^{-2}$ and $1.5 \pm 0.8 \times 10^{-2}$ for Si and PDMS, respectively.

The flexible PDMS replica of the master structure was moulded to the imprinting roller of a PTMTEC (PTMTEC Oy, 00740 Helsinki, Finland) roll-to-roll UV assisted nanoimprinting lithography (R2R UV-NIL) machine. A diagram showing the configuration of the R2R UV-NIL machine combined with the diffractometer can be seen in Fig. 4(a). A flexible substrate is coated by gravure coating with a photo-curable resist (blue) and then moves forward to the imprinting unit, where it is pressed against the soft stamp (attached to the imprinting roller) and cured from the backside

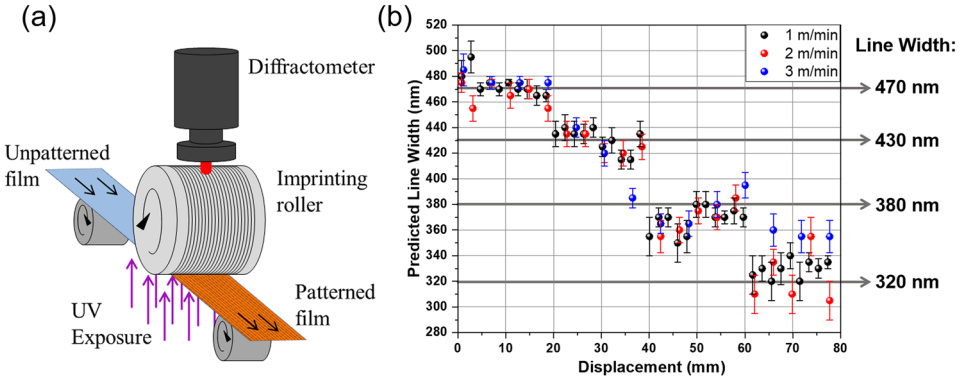

FIG. 4. (a) Schematic diagram showing the configuration of the R2R UV NIL machine combined with the diffractometer, installed to inspect the soft stamp quality. (b) Diffractometry results showing the predicted linewidth after feeding the 4th order intensity peak (with error) into the theoretical calibration curve [Fig. 3(e)] as the soft-stamp is rotated on the imprinting roller in the machine. The experiment was carried out at three different rotation speeds as indicated. The gray arrows represent the four expected linewidth values as measured by SEM.

with UV light. After separation from the stamp, the substrate is successfully patterned (orange). The diffractometer is placed above the imprinting roller to inspect the stamp quality during the imprinting process. Logically any defects in the stamp will be transferred to the patterned film and so is a crucial place for inspection.

Figure S2 of the supplementary material demonstrates the live operation of the in-line diffractometer installed in the R2R UV-NIL system. In this video, the PDMS stamp can be seen attached to the imprinting roller; the measurement head of the diffractometer is installed vertically above, and on the laptop, a live video output from the diffractometry CCD can be seen. When the stamp is rotated past the measurement head, the diffraction pattern can be seen to appear on the screen. Diffractograms were collected with an exposure time of 0.1 ms every 100 ms (frame-rate limited) and post-processed (as described for the static measurements). As a result of such inspection, the intensity of the 4th order diffraction peak and it's fitting error was extracted as a function of the displacement along the imprinting stamp as it is rotated around the roller [Fig. 4(b)]. Additionally, the rotation speed of the roller was altered from 1 to 3 m/min to test the device's capabilities as shown. The output intensities and their associated errors were inputted into the PDMS calibration curve [Fig. 3(e)] resulting in the measured linewidth along the stamp plotted in Fig. 4(b). The same stepwise behavior was observed as for the static silicon master/PDMS stamp; however, the measurement exhibited larger fluctuations within the same grating area. Uncertainty analysis of the data in Fig. 4(b) (shown in Fig. S3 of the supplementary material) reveals an average absolute precision of the R2R measurements of the linewidth to be 10 nm. The relative precision remained relatively constant between the static and R2R measurements [2/3% (Si/PDMS) and 2.5%, respectively] suggesting that there was negligible uncertainty added by vibrations when moving to the R2R system. Fluctuations in the laser intensity (Fig. S4 in the supplementary material) and uncertainty in the SEM measurements of the linewidth, combined, account for 2% of the uncertainty (1% and 1.5%, respectively). The remaining 2% uncertainty needed to match to the experimental precision is put down to the combined fluctuations of the structural height and an uneven surface (therefore changing the angle of incidence). For 1 and 2 m/min roller speed, the measured linewidths were accurate to the expected values from SEM measurements (within the 10 nm precision); however, for 3 m/min, the results on average deviated by up to 20 nm (two standard deviations) away from the expected linewidths.

In summary, an optical diffractometer capable of collecting diffractograms through an aspheric lens in a microscope configuration was demonstrated. This was used as a fast, in-line, and non-invasive method to measure changes in the linewidth of linear silicon gratings. These master structures were then replicated into a soft PDMS stamp, subsequently attached to a R2R UV NIL machine. Two dimensional FDFD simulations were performed and compared to the experimental data and were additionally used to measure the structure height and the angle of incidence in the experiment. The diffractometer was then installed above the rotating soft stamp in order to measure the linewidth of the PDMS stamp in-line to a precision of 10 nm. It is believed that the demonstrated live monitoring process combined with more compressive electromagnetic simulations with multiple diffraction peak analysis, multiple critical dimensions of the gratings can be directly extracted for real-time structural diffractometry.

See supplementary material for statistical outputs for the parametric fits for the χ^2 minimisation, a video of the diffractometer placed above the rotating PDMS stamp in the roll-to-roll system, uncertainty analysis, and laser stability measurements. Figure S1—Histograms of the outputs generated from the χ^2 minimisation technique used to determine the structural parameters of the [(a)–(d)] Si master and [(e)–(h)] the PDMS stamp, where the fitting values were allowed to vary by up to 2 standard deviations. The parameters determined were height [(a)/(e)], the angle of incidence [(b)/(f)], and the corner radius of curvature [(c)/(g)]. It was seen that the height and angle of incidence was degenerated for Si for the given uncertainty of the measurement; however, the PDMS was for the most part singular within the accuracy of the model. [(d)/(h)] Plot the minimum χ^2 achieved for each fitting; Figure S2—Supplementary multimedia figure demonstrating the integration of the diffractometer into the roll-to-roll UV-assisted nanoimprinting system. The optical setup is placed above the PDMS stamp roller to monitor the generated spatial diffraction pattern; Figure S3—(a) the error bars from Fig. 4(b) (absolute precision) plotted with displacement along the rotating stamp and averaged

(b) for each speed with standard deviation shown. (c) The relative precision is achieved by dividing the absolute precision by the predicted linewidth [from Fig. 4(b)] and plotted against displacement and (d) averaged for each speed with the standard deviation shown. (e) The accuracy is calculated by dividing the difference between the measured value from diffractometry and the expected value (from SEM) normalised by absolute precision and (f) the averaged results for each speed; Figure S4—the 4th order diffractive intensity (normalised) measured from the static Si master over 5 min with the standard deviation (1%) of the data shown. The diffraction was generated from the 320 nm linewidth region of the Si master.

The authors acknowledge the financial support from the EU projects, FLEXPOL (No. H2020-NMBP-PILOT-2016-721062), FP7 QUANTIHEAT (No. FP7-NMP-2013-LARGE-7-604668), as well as the MINECO Project PHENTOM (No. FIS2015-70862-P). M.K. acknowledges financial support from the Deutsche Forschungsgemeinschaft (No. KR 4522/1-1). The ICN2 is funded by the CERCA programme/Generalitat de Catalunya. The ICN2 is supported by the Severo Ochoa programme of the Spanish Ministry of Economy, Industry and Competitiveness (MINECO, Grant No. SEV-2013-0295).

[1] M. T. Reetz, M. Maase, T. Schilling, and B. Tesche, J. Phys. Chem. B **104**, 8779 (2000).
[2] L. Gross, Nat. Chem. **3**, 273 (2011).
[3] H. U. Danzebrink, L. Koenders, G. Wilkening, A. Yacoot, and H. Kunzmann, CIRP Ann. **55**, 841 (2006).
[4] L. J. Guo, Adv. Mater. **19**, 495 (2007).
[5] R. K. Leach, R. Boyd, T. Burke, H.-U. Danzebrink, K. Dirscherl, T. Dziomba, M. Gee, L. Koenders, V. Morazzani, A. Pidduck, D. Roy, W. E. S. Unger, and A. Yacoot, Nanotechnology **22**, 62001 (2011).
[6] N. Kooy, K. Mohamed, L. T. Pin, and O. S. Guan, Nanoscale Res. Lett. **9**, 320 (2014).
[7] R. Bogue, Sens. Rev. **27**, 189 (2007).
[8] E. Bugnicourt, T. Kehoe, M. Latorre, C. Serrano, S. Philippe, and M. Schmid, Nanomaterials **6**, 150 (2016).
[9] H. Subbaraman, X. Lin, X. Xu, A. Dodabalapur, L. J. Guo, and R. T. Chen, Proc. SPIE **8466**, 846603 (2012).
[10] P. D. Coates, S. E. Barnes, M. G. Sibley, E. C. Brown, H. G. M. Edwards, and I. J. Scowen, Polymer **44**, 5937 (2003).
[11] M. Wurm, F. Pilarski, and B. Bodermann, Rev. Sci. Instrum. **81**, 023701 (2010).
[12] M. Losurdo, Thin Solid Films **519**, 2575 (2011).
[13] R. M. Al-Assaad, S. Regonda, L. Tao, S. W. Pang, and W. (Walter) Hu, J. Vac. Sci. Technol., B: Microelectron. Nanometer Struct.–Process., Meas., Phenom. **25**, 2396 (2007).
[14] K. Tiede, A. B. A. Boxall, S. P. Tear, J. Lewis, H. David, and M. Hassellov, Food Addit. Contam., Part A **25**, 795 (2008).
[15] C. Raymond, AIP Conf. Proc. **788**, 394–402 (2005).
[16] M. H. Madsen and P. E. Hansen, Surf. Topogr.: Metrol. Prop. **4**, 023003 (2016).
[17] J. S. Madsen, L. H. Thamdrup, I. Czolkos, P. E. Hansen, A. Johansson, J. Garnaes, J. Nygård, and M. H. Madsen, J. Micromech. Microeng. **27**, 085004 (2017).
[18] M. H. Madsen, P.-E. Hansen, M. Zalkovskij, M. Karamehmedović, and J. Garnæs, Optica **2**, 301 (2015).
[19] M. Kreuzer, J. Gomis Bresco, M. Sledzinska, and C. M. Sotomayor-Torres, Proc. SPIE **9628**, 96281Q (2015).
[20] T. Kehoe, V. Reboud, and C. M. Sotomayor-Torres, Microelectron. Eng. **86**, 1036 (2009).
[21] M. Kreuzer, J. Gomis Bresco, M. Sledzinska, and C. M. Sotomayor-Torres, Proc. SPIE **9424**, 942426 (2015).
[22] N. Kumar, O. El Gawhary, S. Roy, V. G. Kutchoukov, S. F. Pereira, W. Coene, and H. P. Urbach, Proc. SPIE **8324**, 83240Q (2012).
[23] O. Gawhary, N. Kumar, S. F. Pereira, W. M. J. Coene, and H. P. Urbach, Appl. Phys. B **105**, 775 (2011).
[24] S. Roy, N. Kumar, S. F. Pereira, and H. P. Urbach, J. Opt. **15**, 075707 (2013).
[25] P. Petrik, N. Kumar, G. Juhasz, C. Major, B. Fodor, E. Agocs, T. Lohner, S. F. Pereira, H. P. Urbach, and M. Fried, J. Phys.: Conf. Ser. **558**, 012008 (2014).
[26] M. Liu, J. Sun, Y. Sun, C. Bock, and Q. Chen, J. Micromech. Microeng. **19**, 35028 (2009).